Direct growth of graphene on in situ epitaxial hexagonal boron nitride flakes by plasma-assisted molecular beam epitaxy

Zhongguang Xu, Renjing Zheng, Alireza Khanaki, Zheng Zuo, and Jianlin Liu

Citation: Applied Physics Letters **107**, 213103 (2015); doi: 10.1063/1.4936378
View online: http://dx.doi.org/10.1063/1.4936378
View Table of Contents: http://scitation.aip.org/content/aip/journal/apl/107/21?ver=pdfcov
Published by the AIP Publishing

Direct growth of graphene on *in situ* epitaxial hexagonal boron nitride flakes by plasma-assisted molecular beam epitaxy

Zhongguang Xu, Renjing Zheng, Alireza Khanaki, Zheng Zuo, and Jianlin Liu[a)]
Quantum Structures Laboratory, Department of Electrical and Computer Engineering, University of California, Riverside, California 92521, USA

(Received 31 August 2015; accepted 10 November 2015; published online 24 November 2015)

Hexagonal boron nitride (h-BN) single-crystal domains were grown on cobalt (Co) substrates at a substrate temperature of 850–900 °C using plasma-assisted molecular beam epitaxy. Three-point star shape h-BN domains were observed by scanning electron microscopy, and confirmed by Raman and X-ray photoelectron spectroscopy. The h-BN on Co template was used for *in situ* growth of multilayer graphene, leading to an h-BN/graphene heterostructure. Carbon atoms preferentially nucleate on Co substrate and edges of h-BN and then grow laterally to form continuous graphene. Further introduction of carbon atoms results in layer-by-layer growth of graphene on graphene and lateral growth of graphene on h-BN until it may cover entire h-BN flakes. © *2015 AIP Publishing LLC*. [http://dx.doi.org/10.1063/1.4936378]

Hexagonal boron nitride (h-BN) currently attracts considerable attentions both for its fascinating properties of the individual monolayer and successful incorporation as a complementary two-dimensional dielectric substrate in graphene based electronics from experimental and theoretical work.[1–12] H-BN has a crystal lattice structure similar to that of graphene with less than 2% lattice mismatch.[13] In addition, it is a wide band gap (~5.9 eV) III-V compound with remarkable physical and chemical properties, such as high chemical inertness, high temperature stability, low dielectric constant, large thermal conductivity, and high mechanical strength.[4–6] So far, many methods have been used to obtain atomic h-BN films, such as micromechanical cleavage,[14,15] liquid sonication,[16] and chemical vapor deposition (CVD).[4–8] Recently, we have synthesized large single-crystalline h-BN domains and continuous wafer-scale h-BN thin films on epitaxial graphene using plasma-assisted molecular beam epitaxy (MBE).[17] This result serves as an important first step toward functional nanoelectronic devices based on graphene/h-BN heterostructures. To further enhance processing and integration capability of graphene/h-BN heterostructures for various devices, it is essential to reliably grow graphene on h-BN as well. CVD has already been used to grow single-domain graphene on exfoliated h-BN.[18,19] Recently, Gao *et al*. reported in-plane and vertically epitaxial growth of graphene on h-BN using benzoic acid precursor on Cu substrate in a CVD system.[20] Nevertheless, direct deposition of high-quality graphene on *in situ* epitaxial h-BN remains challenging.

In this paper, we report our results of epitaxial growth of two-dimensional h-BN flakes on Co substrate and growth of wafer-scale graphene on these h-BN flakes using plasma-assisted MBE. Various characterizations have been performed to assess these films, and the growth mechanism is discussed.

First, an E-beam evaporation system was used to grow Co film of 400 nm on a 300-nm-thick SiO_2 coated Si (100) substrate. The substrate of 1 cm × 1 cm was cut from the wafer and transferred into an MBE chamber. A Knudsen effusion cell filled with B_2O_3 powder (Alfa Aesar, 99.999%) was used as boron (B) source. A thermocracker was used to crack acetylene gas (Airgas, 99.999%) as carbon (C) source. An electron cyclotron resonance (ECR) system was used to generate nitrogen plasma (Airgas, 99.9999%) as nitrogen (N) source.

For the growth of h-BN (Sample A), the substrate was firstly annealed at 900 °C under a hydrogen flow rate of 10 sccm for a duration of 60 min. Then, the hydrogen gas flow rate was decreased to 6 sccm, and h-BN was grown at a B cell temperature of 1050 °C and a nitrogen flow rate of 10 sccm. The ECR current was set at 60 mA with a power of 228 W. The growth lasted for 15 min. During the growth of h-BN/graphene stacked layer (Sample B), the h-BN part was grown with a similar growth condition as that of the reference Sample A, except that the substrate temperature was kept at 850 °C and B cell temperature was 1000 °C. Graphene was subsequently grown at an acetylene flow rate of 3 sccm through the thermocracker heated at 1200 °C for 30 s. Finally, the substrate was cooled down to room temperature at a rate of 10 °C/min.

Raman characterizations were performed using a HORIBA LabRam system equipped with a 50-mW 514-nm green laser. Scanning electron microscope (SEM) images were acquired using an XL30-FEG system. X-ray photoelectron spectroscopy (XPS) was carried out using a Kratos AXIS ULTRA XPS system equipped with an Al Kα monochromatic X-ray source and a 165 mm mean radius electron energy hemispherical analyzer. Atomic force microscope (AFM) images were obtained using a Veeco AFM D3100 system.

Fig. 1(a) shows an SEM image of h-BN sample (Sample A) obtained in secondary electron imaging mode. As seen from the image, three-point star shape h-BN domains of ~1 μm are evident, which are different from the perfect

[a)]Author to whom correspondence should be addressed. Electronic mail: jianlin@ece.ucr.edu

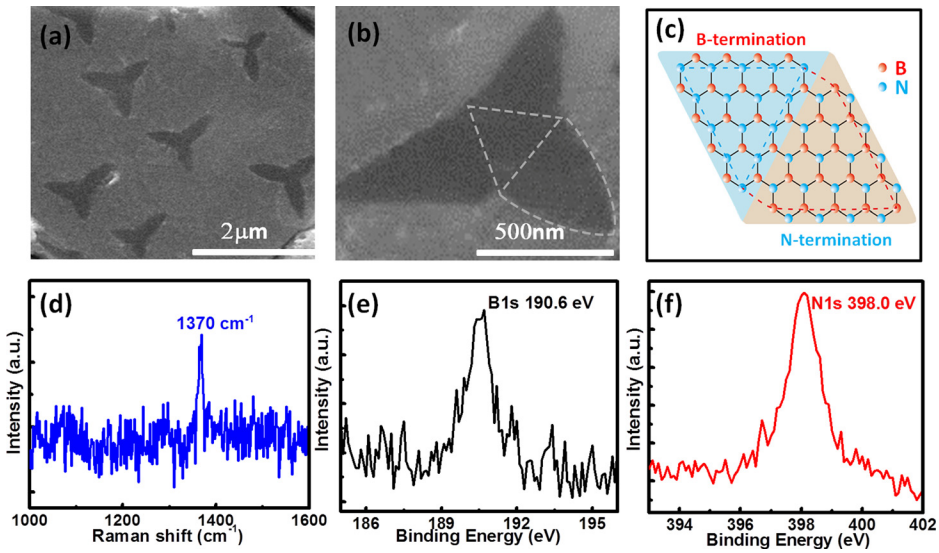

FIG. 1. (a) SEM image of as grown h-BN domains on Co substrate (Sample A), (b) magnified SEM image of one single h-BN domain, (c) schematic illustration of a possible atom arrangement scheme of the three-point star shape domains. (d) Raman spectrum of Sample A. A peak located at 1370 cm^{-1} is observed, relating to E_{2g} optical phonon peak of h-BN, (e) B1s XPS, and (f) N1s XPS spectra of Sample A. B1s peak and N1s peak are at 190.6 eV, and 398.0 eV, respectively, indicating the existence of h-BN.

triangular shape of the h-BN domains grown on Cu foil and Ni (111) by CVD.[7,21,22] Fig. 1(b) shows a magnified SEM image of a typical three-point star shape h-BN domain. Each three-point star shape h-BN domain is composed of a central triangle and three sharp triangles at its edge. Visualization of any one of the sharp triangles together with its central triangle, which is marked using dashed lines in the image, gives a "diamond shape" area. Similar results have been also observed for h-BN domains in CVD process[7] and in other epitaxial two dimensional materials, such as MoS_2[23] and WS_2.[24] Fig. 1(c) shows a schematic of a possible mechanism, which indicates that a nitrogen-terminated triangular shape region connects another boron-terminated triangle back-to-back.[7] From theoretical calculations,[21,25] the nitrogen-terminated triangles have lower edge energy than that of the boron-terminated ones, which suggests that nitrogen-terminated h-BN flakes would be energetically favorable. Therefore, it is likely that the central triangle is boron-terminated while the edges of the three surrounding triangles are nitrogen-terminated. Fig. 1(d) shows Raman spectrum of Sample A. A Raman peak at 1370 cm^{-1} is observed, which is corresponding to the E_{2g} vibration mode of h-BN and indicates the h-BN film is monolayer.[26–28] Very small full width at half maximum (FWHM) of the peak (15 cm^{-1}) suggests that the h-BN is of high quality. Figs. 1(e) and 1(f) show XPS spectrum of B1s and N1s state of the sample, respectively. B1s and N1s exhibit an energy position at 190.6 eV and 398.0 eV, respectively, which are typical characteristics of h-BN.[5,29] Based on the integrated peak intensity, B/N ratio was estimated to be 1:1.03. It means that the compositions of B and N elements are almost equal, indicating that h-BN domains are stoichiometric.

Figs. 2(a) and 2(b) show a typical optical microscope image and an SEM image of as grown h-BN/graphene heterostructure (Sample B), respectively. Both images show continuous as grown film, however, color non-uniformity is evident in the images, indicating that the thickness of respective graphene and h-BN layers varies across these imaging areas of the sample. This is a reasonable result from the fact that h-BN is not a continuous film but consists of discrete

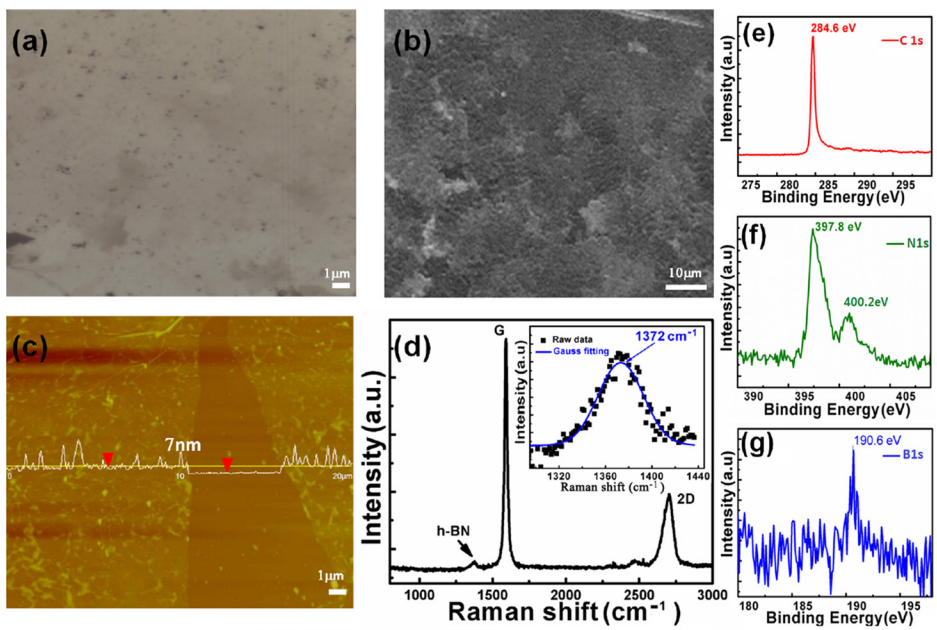

FIG. 2. (a) Optical microscope image, and (b) SEM image of as grown h-BN/graphene stacked structure (Sample B), (c) AFM image of a transferred h-BN/graphene structure on SiO_2, (d) Raman spectrum of a transferred h-BN/graphene structure on SiO_2. The G/2D peak ratio of graphene indicates the existence of multi-layer graphene. H-BN peak is observed besides G peak. The inset zooms in h-BN peak of 1372 cm^{-1}, relating to E_{2g} optical phonon peak of h-BN, (e)–(g) XPS spectra of C1s, N1s, and B1s peaks.

flakes on the Co substrate. Fig. 2(c) shows an AFM image of a transferred h-BN/graphene heterostructure, which was transferred onto a SiO_2 substrate using a similar transfer process described in Ref. 5. The height profile of a scanned line indicates that the h-BN/graphene has a thickness of ~7 nm on average. Fig. 2(d) shows Raman spectrum of the transferred sample. The G/2D peak ratio of the graphene signals indicates the existence of multi-layer graphene. An evident peak is also observed at 1372 cm^{-1}, which is corresponding to h-BN E_{2g} optical phonon mode. Moreover, there is no graphene D peak, indicating high-quality graphene film. Figs. 2(e)–2(g) show XPS spectra of C1s, N1s, and B1s, respectively. C1s peak at 284.6 eV originates from sp^2 C-C bond,[30] which is an indication of the formation of graphene. B1s and N1s exhibit energy positions at 190.6 eV and 397.8 eV, respectively, which are consistent with previous reports of these XPS characteristic lines of h-BN.[5,30] Moreover, a weak peak at 400.2 eV is observed in Fig. 2(f), which originates from N-C bonding.[31] The N–C bonding indicates the existence of in-plane hybridization of graphene and h-BN in the heterostructures and further confirms that the h-BN flakes have nitrogen-terminated edges.

Figs. 3(a) and 3(b) show Raman mapping result of Sample B for h-BN E_{2g} peak and graphene G peak from one area on the sample, respectively. The insets in (a) and (b) show Raman spectrum of the spots indicated by squares on the image, respectively. It is evident that graphene covers all mapped area, while h-BN Raman signal is found sporadically on the mapped area. It indicates that graphene has grown across these h-BN flakes. Figs. 3(c) and 3(d) show Raman mapping result for h-BN E_{2g} peak and graphene G peak on another area on the sample where there is a larger h-BN flake, respectively. As seen from the image in Fig. 3(c), graphene has not been formed on the h-BN flake. Further careful study of the boundary between the graphene and h-BN leads to an identification of three regions A, B, and C, which are marked on Fig. 3(d). Each region manifests its representative Raman spectrum, as shown in the inset. Region A and C show pure h-BN and graphene, respectively, while the boundary region (Region B) exhibits both h-BN and graphene signals.

Finally, we briefly discuss a phenomenological growth mechanism based on the above experimental results, which is schematically shown in Fig. 4. At the beginning, boron atoms and activated nitrogen atoms impinge on the Co substrate surface to form h-BN flakes (Fig. 4(a)). After the growth of h-BN flakes, carbon atoms are introduced and graphene starts to nucleate both on the Co surface[32,33] and at the edges of h-BN flakes[34,35] since these edges serve as perfect atomic steps (Fig. 4(b)). The nucleation of graphene on these defect-free surfaces of h-BN flakes is relatively slow. Although the mechanism is still poorly understood, there are experimental findings that the growth of single-layer graphene on h-BN would take a few hours.[17,18,36] Then graphene grows laterally to connect each other to form continuous film (Fig. 4(c)). Further introduction of carbon atoms leads to the layer-by-layer growth of graphene on graphene and further lateral growth of graphene on uncovered h-BN (Fig. 4(d)). For those small h-BN flakes, graphene can grow across them resulting in h-BN/graphene stacked heterostructures, while for larger flakes, longer graphene growth time is necessary for the entire flakes to be covered. It suggests that the size of h-BN flakes have played a key factor on graphene growth across h-BN flakes.

We demonstrated h-BN epitaxial growth on Co substrate by plasma-assisted MBE. Three-point star shape h-BN domains were observed. Based on h-BN growth, we also achieved direct epitaxial growth of h-BN/graphene heterostructures with atomic multi layers. It is found that graphene starts to nucleate on the Co substrate and edges of h-BN flakes, and then grows across h-BN flakes to form local h-BN/graphene heterostructures. Due to negligible nucleation rate of graphene

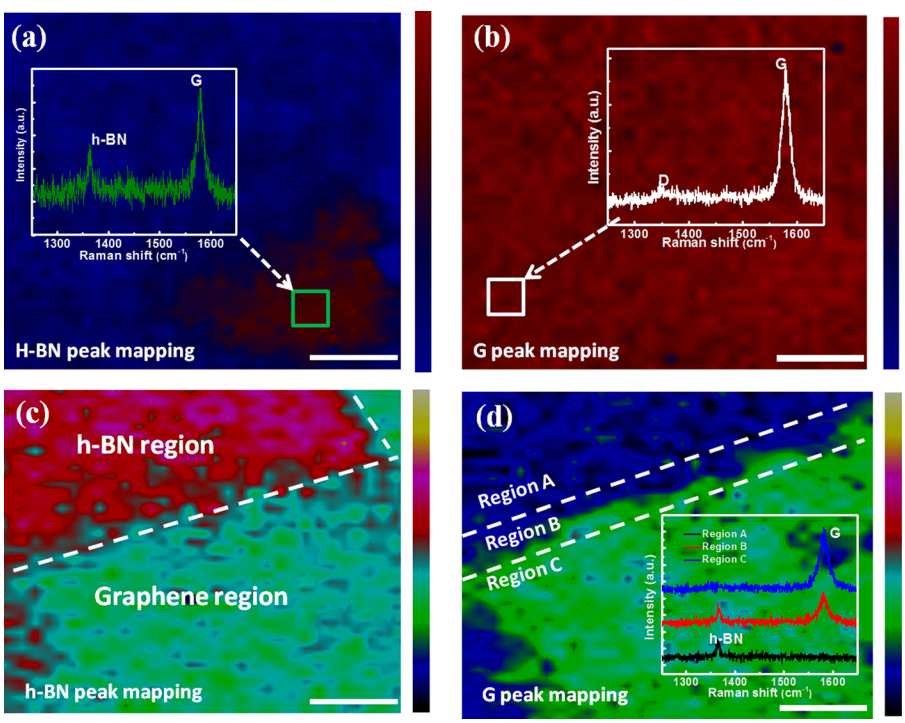

FIG. 3. Raman mapping of Sample B for (a) h-BN E_{2g} peak of h-BN, and (b) graphene G peak at one surface area, and (c) h-BN E_{2g} peak and (d) graphene G peak at another surface area. Insets show Raman spectra accordingly. All scale bars are 1 μm.

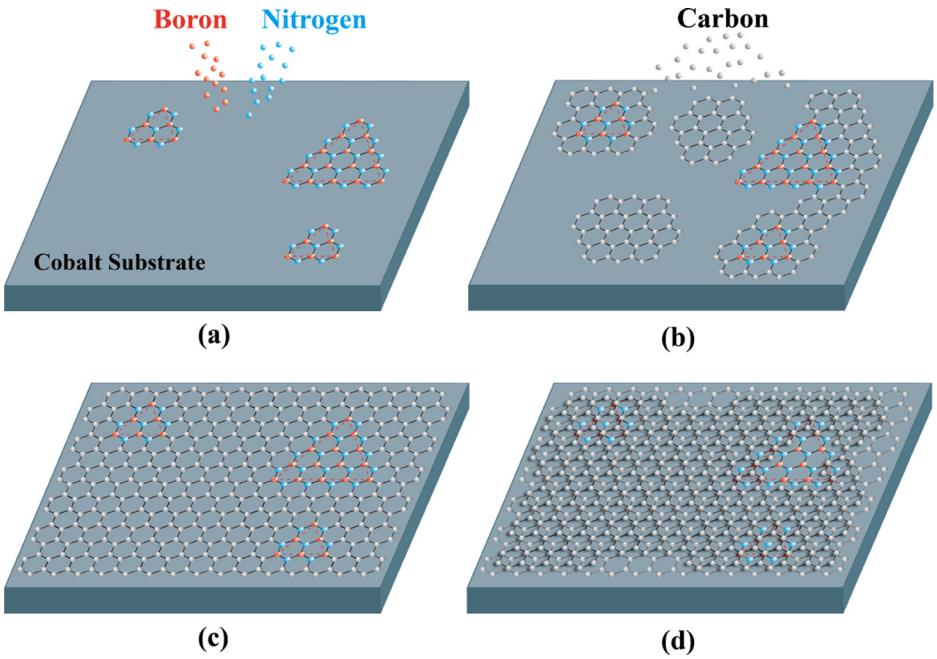

FIG. 4. Schematic of growth mechanism for the MBE growth of h-BN/graphene heterostructure on Co substrate. (a) h-BN nucleation on Co substrate, (b) initial graphene nucleation on Co substrate and edges of h-BN flakes, (c) lateral growth of graphene, and (d) layer-by-layer graphene growth on graphene and lateral graphene growth on h-BN flakes.

on the surface of h-BN compared with those on the Co substrate and edges of h-BN, larger h-BN flakes are only partially covered by graphene near the edge areas due to lateral graphene growth under a short growth process.

We thank Mr. Xiaoxiong Ding for his assistance in schematic drawing. This work was supported by FAME, one of six centers of STARnet, a Semiconductor Research Corporation program supported by MACRO and DARPA.

[1]Z. Liu, L. Ma, G. Shi, W. Zhou, Y. Gong, S. Lei, X. Yang, J. Zhang, J. Yu, K. P. Hackenberg, A. Babakhani, J-C. Idrobo, R. Vajtai, J. Lou, and P. M. Ajayan, Nat. Nanotechnol. **8**, 119 (2013).
[2]A. Nag, K. Raidongia, R. Datta, K. P. S. S. Hembaram, U. V. Waghmare, and C. N. Rao, ACS Nano **4**, 1539 (2010).
[3]C. Dean, A. Young, I. Meric, C. Lee, L. Wang, S. Sorgenfrei, K. Watanabe, T. Taniguchi, P. Kim, K. L. Shepard, and J. Hone, Nat. Nanotechnol. **5**, 722 (2010).
[4]Z. Liu, L. Song, S. Zhao, J. Huang, L. Ma, J. Zhang, J. Lou, and P. M. Ajayan, Nano. Lett. **11**, 2032 (2011).
[5]L. Song, L. Ci, H. Lu, P. Sorokin, C. Jin, J. Ni, A. Kvashnin, D. Kvashnin, J. Lou, B. Yakobson, and P. Ajayan, Nano Lett. **10**, 3209 (2010).
[6]Y. Shi, C. Hamsen, X. Jia, K. Kim, A. Reina, M. Hofmann, A. Hsu, K. Zhang, H. Li, Z. Juang, M. Dresselhaus, L. Li, and J. Kong, Nano Lett. **10**, 4134 (2010).
[7]K. Kim, A. Hsu, X. Jia, S. Kim, Y. Shi, M. Hofmann, D. Nezich, J. Rodriguez-Nieva, M. Dresselhaus, T. Palacios, and J. Kong, Nano Lett. **12**, 161 (2012).
[8]G. Kim, A. Jang, H. Y. Jeong, Z. Lee, D. Kang, and H. Shin, Nano Lett. **13**, 1834 (2013).
[9]R. Balu, X. Zhong, R. Pandey, and S. P. Karna, Appl. Phys. Lett. **100**, 052104 (2012).
[10]T. P. Kaloni, Y. C. Cheng, and U. Schwingenschlögl, J. Mater. Chem. **22**, 919 (2012).
[11]P. Moon and M. Koshino, Phys. Rev. B **90**, 155406 (2014).
[12]A. Principi, M. Carrega, M. B. Lundeberg, A. Woessner, F. H. L. Koppens, G. Vignale, and M. Polini, Phys. Rev. B **90**, 165408 (2014).
[13]G. Giovannetti, P. Khomyakov, G. Brocks, P. Kelly, and J. Brink, Phys. Rev. B **76**, 073103 (2007).
[14]K. S. Novoselov, D. Jiang, F. Schedin, T. J. Booth, V. V. Khotkevich, S. V. Morozov, and A. K. Geim, Proc. Natl. Acad. Sci. U.S.A. **102**, 10451 (2005).
[15]D. Pacilé, J. C. Meyer, Ç. Ö. Girit, and A. Zettl, Appl. Phys. Lett. **92**, 133107 (2008).
[16]J. N. Coleman, M. Lotya, A. O'Neill, S. D. Bergin, P. J. King, U. Khan, K. Young, A. Gaucher, S. De, R. J. Smith, I. V. Shvets, S. K. Arora, G. Stanton, H.-Y. Kim, K. Lee, G. T. Kim, G. S. Duesberg, T. Hallam, J. J. Boland, J. J. Wang, J. F. Donegan, J. C. Grunlan, G. Moriarty, A. Shmeliov, R. J. Nicholls, J. M. Perkins, E. M. Grieveson, K. Theuwissen, D. W. McComb, P. D. Nellist, and V. Nicolosi, Science **331**, 568 (2011).
[17]Z. Zuo, Z. Xu, R. Zheng, A. Khanaki, J. Zheng, and J. Liu, Sci. Rep. **5**, 14760 (2015).
[18]X. Ding, G. Ding, X. Xie, F. Huang, and M. Jiang, Carbon **49**, 2522 (2011).
[19]W. Yang, G. Chen, Z. Shi, C. Liu, L. Zhang, G. Xie, M. Cheng, D. Wang, R. Yang, D. Shi, K. Watanabe, T. Taniguchi, Y. Yao, Y. Zhang, and G. Zhang, Nat. Mater. **12**, 792 (2013).
[20]T. Gao, X. Song, H. Du, Y. Nie, Y. Chen, Q. Ji, J. Sun, Y. Yang, Y. Zhang, and Z. Liu, Nat. Commun. **6**, 6835 (2015).
[21]W. Auwarter, H. Suter, H. Sachdev, and T. Greber, Chem. Mater. **16**, 343 (2004).
[22]Y. Roland, H. Mark, M. Govind, H. Siu, S. Ram, T. Travis, H. Edwin, and P. Shashi, Nano Lett. **14**, 839 (2014).
[23]A. M. van der Zande, P. Y. Huang, D. A. Chenet, T. C. Berkelbach, Y. You, G. H. Lee, T. F. Heinz, D. R. Reichman, D. A. Muller, and J. C. Hone, Nat. Mater. **12**, 554 (2013).
[24]C. Cong, J. Shang, X. Wu, B. Cao, N. Peimyoo, C. Qiu, L. Sun, and T. Yu, Adv. Opt. Mater. **2**, 131 (2014).
[25]Y. Liu, S. Bhowmick, and B. Yakobson, Nano Lett. **11**, 3113 (2011).
[26]R. Gorbachev, I. Riaz, R. Nair, R. Jali, L. Britnell, B. Belle, E. Hill, K. Novoselov, K. Watanabe, T. Taniguchi, A. Geim, and P. Blake, Small **7**, 465 (2011).
[27]J. Han, J.-Y. Lee, H. Kwon, and J.-S. Yeo, Nanotechnology **25**, 145604 (2014).
[28]H. Zhou, J. Zhu, Z. Liu, Z. Yan, X. Fan, J. Lin, G. Wang, Q. Yan, T. Yu, P. Ajayan, and J. M. Tour, Nano Res. **7**, 1232 (2014).
[29]K. Park, D. Lee, K. Kim, and D. Moon, Appl. Phys. Lett. **70**, 315 (1997).
[30]E. Moreau, F. Ferrer, D. Vignaud, S. Godey, and S. Wallart, Phys. Status Solidi A **207**, 300 (2010).
[31]C. Zhang, S. Zhao, C. Jin, A. L. Koh, Y. Zhou, W. Xu, Q. Li, Q. Xiong, H. Peng, and Z. Liu, Nat. Commun. **6**, 6519 (2015).
[32]N. Zhan, G. Wang, and J. Liu, Appl. Phys. A **105**, 341 (2011).
[33]E. Kim, H. An, H. Jang, W. Cho, N. Lee, W. Lee, and J. Jung, Chem. Vap. Deposition **17**, 9 (2011).
[34]L. Liu, J. Park, D. A. Siegel, K. F. McCarty, K. W. Clark, W. Deng, L. Basile, J. Idrobo, A. Li, and G. Gu, Science **343**, 163 (2014).
[35]M. Liu, Y. Li, P. Chen, J. Sun, D. Ma, Q. Li, T. Gao, Y. Gao, Z. Cheng, X. Qiu, Y. Fang, Y. Zhang, and Z. Liu, Nano Lett. **14**, 6342 (2014).
[36]J. M. Garcia, U. Wurstbauer, A. Levy, L. N. Pfeiffer, A. Pinczuk, A. S. Plaut, L. Wang, C. R. Dean, R. Buizza, A. M. Van Der Zande, J. Hone, K. Watanabe, and T. Taniguchi, Solid State Commun. **152**, 975 (2012).